

A systematic search for transiting planets in the *K2* data

Daniel Foreman-Mackey^{1,2}, Benjamin T. Montet^{3,4}, David W. Hogg^{2,5,6},
Timothy D. Morton⁷, Dun Wang², & Bernhard Schölkopf⁸

ABSTRACT

Photometry of stars from the *K2* extension of NASA's *Kepler* mission is afflicted by systematic effects caused by small (few-pixel) drifts in the telescope pointing and other spacecraft issues. We present a method for searching *K2* light curves for evidence of exoplanets by simultaneously fitting for these systematics and the transit signals of interest. This method is more computationally expensive than standard search algorithms but we demonstrate that it can be efficiently implemented and used to discover transit signals. We apply this method to the full Campaign 1 dataset and report a list of 36 planet candidates transiting 31 stars, along with an analysis of the pipeline performance and detection efficiency based on artificial signal injections and recoveries. For all planet candidates, we present posterior distributions on the properties of each system based strictly on the transit observables.

Subject headings: methods: data analysis — methods: statistical — catalogs — planetary systems — stars: statistics

¹To whom correspondence should be addressed: danfm@nyu.edu

²Center for Cosmology and Particle Physics, Department of Physics, New York University, 4 Washington Place, New York, NY, 10003, USA

³Cahill Center for Astronomy and Astrophysics, California Institute of Technology, Pasadena, CA, 91125, USA

⁴Harvard-Smithsonian Center for Astrophysics, Cambridge, MA 02138, USA

⁵Max-Planck-Institut für Astronomie, Königstuhl 17, D-69117 Heidelberg, Germany

⁶Center for Data Science, New York University, 726 Broadway, 7th Floor, New York, NY, 10003, USA

⁷Department of Astrophysics, Princeton University, Princeton, NJ, 08544, USA

⁸Max Planck Institute for Intelligent Systems, Spemannstrasse 38, 72076 Tübingen, Germany

1. Introduction

The *Kepler* Mission was incredibly successful at finding transiting exoplanets in the light curves of stars. The Mission has demonstrated that it is possible to routinely measure signals in stellar light curves at the part-in- 10^5 level. Results from the primary mission include the detection of planet transits with depths as small as 12 parts per million (Barclay et al. 2013).

The noise floor for *Kepler* data is often quoted as 15 parts per million (ppm) per six hours of observations (Gilliland et al. 2011). Although they generally do not interfere with searches for transiting planets, larger systematic effects exist on different timescales. One of the most serious of these is spacecraft pointing: If the detector flat-field is not known with very high accuracy, then tiny changes to the relative illumination of pixels caused by a star’s motion in the focal plane will lead to changes in the measured or inferred brightness of the star.

The great stability of the original *Kepler* Mission came to an end with the failure of a critical reaction wheel. The *K2* Mission (Howell et al. 2014) is a follow-on to the primary Mission, observing about a dozen fields near the ecliptic plane, each for ~ 75 days at a time. Because of the degraded spacecraft orientation systems, the new *K2* data exhibit far greater pointing variations—and substantially more pointing-induced variations in photometry—than the original *Kepler* Mission data. This makes good data-analysis techniques even more valuable.

Good photometry relies on either a near-perfect flat-field and pointing model or else data-analysis techniques that are insensitive to these instrument properties. The flat-field for *Kepler* was measured on the ground before the launch of the spacecraft, but is not nearly as accurate as required to make pointing-insensitive photometric measurements at the relevant level of precision. In principle direct inference of the flat-field might be possible; however, because point sources are observed with relatively limited spacecraft motion, and only a few percent of the data are actually stored and downloaded to Earth, there isn’t enough information in the data to derive or infer a complete or accurate flat-field map. Therefore, work on *K2* is sensibly focused on building data-analysis techniques that are pointing-insensitive.

Previous projects have developed methods to work with *K2* data. Both Vanderburg & Johnson (2014) and Armstrong et al. (2014) extract aperture photometry from the pixel data and decorrelate with image centroid position, producing light curves for each star that are “corrected” for the spacecraft motion. These data have produced the first confirmed planet found with *K2* (Vanderburg et al. 2014). Both Aigrain et al. (2015) and Crossfield et al.

(2015) use a Gaussian Process model for the measured flux, with pointing measurements as the inputs, and then “de-trend” using the mean prediction from that model. Other data-driven approaches have been developed and applied to the data from space missions (for example, Ofir et al. 2010; Stumpe et al. 2012; Smith et al. 2012; Petigura et al. 2013a; Wang et al. 2015) and ground-based surveys (for example, Kovács et al. 2005; Tamuz et al. 2005; Berta et al. 2012) but they have yet to be generalized to *K2*.

In all of these light-curve processing methodologies, the authors follow a traditional procedure of “correcting” or “de-trending” the light curve to remove systematic and stellar variability as a step that happens *before* the search for transiting planets. Fit-and-subtract is dangerous: Small signals, such as planet transits, can be partially absorbed into the best-fit stellar variability or systematics models, making each individual transit event appear shallower. In other words, the traditional methods are prone to over-fitting. Because over-fitting will in general reduce the amplitude of true exoplanet signals, small planets that ought to appear just above any specific signal-to-noise or depth threshold could be missed because of the de-trending. This becomes especially important as the amplitude of the noise increases.

The alternative to this approach is to *simultaneously fit* both the systematics and the transit signals. Simultaneous fitting can push the detection limits to lower signal-to-noise while robustly accounting for uncertainties about the systematic trends. In particular, it permits us to *marginalize* over choices in the noise model and propagate any uncertainties about the systematic effects to our confidence in the detection. This marginalization ensures that any conclusions we come to about the exoplanet properties are conservative, given the freedom of the systematics model.

In this *Article* we present a data-analysis technique for exoplanet search and characterization that is insensitive to spacecraft-induced trends in the light curves. We assume that the dominant trends in the observed light curves in each star are caused by the spacecraft and are, therefore, shared with other stars. We reduce the dimensionality by running PCA on stellar light curves to obtain the dominant modes. The search for planets proceeds by modeling the data as a linear combination of 150 of these basis vectors and a transit model. Our method builds on the ideas behind previous data-driven de-trending procedures such as the *Kepler* pipeline pre-search data conditioning (*PDC*; Stumpe et al. 2012; Smith et al. 2012), but (because of our simultaneous fitting approach) we can use a much more flexible systematics model while being less prone to over-fitting.

The methods developed within this paper are highly relevant to both *K2* and the upcoming *TESS* mission (Ricker et al. 2014). *TESS* will feature pointing precision of ~ 3 arc-

seconds¹, similar to the level of pointing drift with *K2*. Moreover, the typical star will be only observed for one month at a time, and the typical transit detection will be at a similar signal-to-noise ratio as with *K2*.

Catalogs of transiting planets found in the *K2* data will be important to better understand the physical properties, formation, and evolution of planetary systems. These planets, especially when they orbit bright or late-type stars, will be useful targets for ground-based and space-based follow-up, both for current facilities and those planned in the near future such as *JWST*. They will also deliver input data for next-generation population inferences (Foreman-Mackey et al. 2014), especially for the population of planets around cool stars (for example, Dressing & Charbonneau 2015).

This project follows in the tradition of independently implemented transit search algorithms applied to publicly available datasets (such as Petigura et al. 2013b,a; Sanchis-Ojeda et al. 2014; Dressing & Charbonneau 2015). These efforts have been hugely successful, especially in the field of exoplanet population inference because, thanks to their relative simplicity, the efficiency and behavior of these pipelines can be quantified empirically. The work described in this *Article* is built on many of the same principles as the previous projects developed for studying *Kepler* data but our main intellectual contribution is a computationally tractable framework for simultaneously fitting for the trends and the transit signal even when searching for planets.

The *Article* is organized as follows. In Section 2, we describe our method of extracting aperture photometry from the calibrated *K2* postage stamp time series. In Section 3 (with details in Appendix A), we describe our data-driven model for the systematic trends in the photometric light curves and our method for fitting this model simultaneously with a transit signal. In Section 4, we give the detailed procedure that we use for discovering and vetting planet candidates. To quantify the performance and detection efficiency of our pipeline, we test (in Section 5) the recovery of synthetic transit signals, spanning a large range of physical parameters, injected into real *K2* light curves. Finally, in Section 6, we present a catalog of 36 planet candidates orbiting 31 stars from the publicly available *K2* Campaign 1 dataset.

¹http://tess.gsfc.nasa.gov/documents/TESS_FactSheet_Oct2014.pdf

2. Photometry and Eigen Light Curves

The starting point for analysis is the raw pixel data. We download the full set of 21,703 target pixel files for *K2*’s Campaign 1 from MAST². We extract photometry using fixed, approximately circular, binary apertures of varying sizes centered on the predicted location of the target star based on the world coordinate system. For each target, we use a set of apertures ranging in radius from 1 to 5 pixels (in steps of 0.5 pixels). Following [Vanderburg & Johnson \(2014\)](#), we choose the aperture size with the minimum CDPP ([Christiansen et al. 2012](#)) with a 6 hour window.³

All previous methods for analyzing *K2* data involve some sort of “correction” or “de-trending” step based on measurements of the pointing of the spacecraft ([Vanderburg & Johnson 2014](#); [Aigrain et al. 2015](#); [Crossfield et al. 2015](#)). In our analysis, we do not do any further preprocessing of the light curves because, as we describe in the next Section, we fit raw photometric light curves with a model that includes both the trends and the transit signal.

One key realization that is also exploited by the official *Kepler* pipeline is that the systematic trends caused by pointing shifts and other instrumental effects are shared—with different signs and weights—by all the stars on the focal plane. For a rigorous theoretical analysis of this problem, see ([Schölkopf et al. 2015](#)). To capitalize on this, the *PDC* component of the *Kepler* pipeline removes any trends from the light curves that can be fit using a linear combination of a small number of “co-trending basis vectors”. This basis of trends was found by running Principal Component Analysis (PCA) on a large set of (filtered) light curves and extracting the top few (~ 4) components ([Stumpe et al. 2012](#); [Smith et al. 2012](#)). Similarly, we ran PCA on the full set of our own generated *K2* Campaign 1 light curves to determine a basis of representative trends but, unlike *PDC*, we retain and use a larger number of these components (150). For clarity, we will refer to our basis as a set of “eigen light curves” (ELCs) and the full set is made available online⁴. The top ten ELCs for Campaign 1 are shown in Figure 1.

²<https://archive.stsci.edu/k2/>

³Note that although we chose a specific aperture for each star, photometry for every aperture radius is available online: <http://bbq.dfm.io/ketu>.

⁴<http://bbq.dfm.io/ketu>

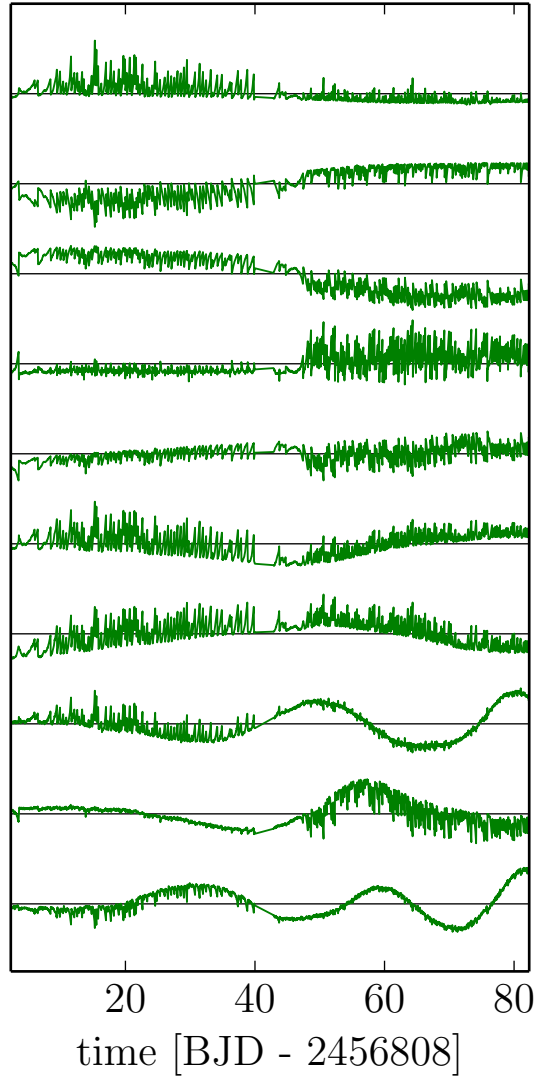


Fig. 1.— The top 10 eigen light curves (ELCs) generated by running principal component analysis on all the aperture photometry from Campaign 1.

3. Joint transit & variability model

The key insight in our transit search method that sets it apart from most standard procedures is that no de-trending is necessary. Instead, we can fit for the noise (or trends) and exoplanet signals simultaneously. This is theoretically appealing because it should be more sensitive to low signal-to-noise transits and similar methods have been shown to be effective for finding transits in ground-based surveys (Berta et al. 2012). The main motivation for this model is that the signal is never precisely orthogonal to the systematics and any de-trending will over-fit. This will, in turn, decrease the amplitude of the signal and distort its shape. In order to reduce these effects, most de-trending procedures use a very rigid model for the systematics. For *K2*, this rigidity has been implemented by effectively asserting that centroid measurements contain all of the information needed to describe the trends (Vanderburg & Johnson 2014; Aigrain et al. 2015; Crossfield et al. 2015). In the *Kepler* pipeline, this is implemented by allowing only a small number of PCA components to contribute to the fit in the *PDC* procedure. Instead, we will use a large number of ELCs—a very flexible model—and use a simultaneous fitting and marginalization to avoid over-fitting.

Physically, the motivation for our model—and the *PDC* model—is that every star on the detector should be affected by the same set of systematic effects. These are caused by things like pointing jitter, temperature variations, and other sources of PSF modulation. Each of these effects will be imprinted in the light curves of many stars with varying amplitudes and signs as a result of the varying flat field and PSF. Therefore, while it is hard to write down a physical generative model for the systematics, building a data-driven model might be possible. This intuition is also exploited by other methods that model the systematics using only empirical centroids (Vanderburg & Johnson 2014; Armstrong et al. 2014; Aigrain et al. 2015; Crossfield et al. 2015), but our more flexible model should capture a wider range of effects, including those related to PSF and temperature. For example, Figure 2 shows the application of our model—with 150 ELCs—to a light curve with no known transit signals and the photometric precision is excellent.

If we were to apply this systematics model alone (without a simultaneous fit of the exoplanet transit model) to a light curve with transits, we would be at risk of over-fitting and decreasing the amplitude of the signal. Figure 3 demonstrates this effect on a synthetic transit injected into the light curve of a typical bright star. The middle two panels in this Figure show the light curve de-trended using 10 and 150 ELCs respectively. When only 10 ELCs are used, the measured transit depth is relatively robust but this model is clearly not sufficient for removing the majority of the systematic trends. The model with 150 ELCs does an excellent job of removing the systematics but it also distorts the transit shape and decreases the measured transit depth, hence reducing the signal strength in the *BLS*

spectrum (Kovács et al. 2002).

In our pipeline we simultaneously fit for the transit signal and the trends using a rigid model for the signal and a relatively flexible model for the systematic noise. Specifically, we model the light curve as being generated by linear combination of 150 ELCs and a “box” transit model at a specific period, phase, and duration. The mathematical details are given in Appendix A, but in summary, since the model is linear, we can analytically compute the likelihood function—conditioned on a specific period, phase, and duration—for the depth *marginalizing out the parameters of the systematics model*. The signal-to-noise of this depth measurement can then be used as a quality of fit metric or candidate selection scalar. This computation is expensive but, as described in the following Sections, it is possible to scale the method to a *K2*-size dataset. The bottom panel of Figure 3 shows the application of this joint transit–systematics model to the synthetic transit discussed previously. When the joint model is used, the correct transit depth is measured—the transit is not distorted—but the systematics are also well-described by the model.

It is worth noting that this model can be equivalently thought of as a (computationally expensive) generalization of the “Box Least Squares” (*BLS*; Kovács et al. 2002) method to a more sophisticated description of the noise and systematics. Therefore, any existing search pipeline based on *BLS* could, in theory, use this model as a drop-in replacement, although some modifications might be required for computational tractability.

The choice to use 150 basis functions is largely arbitrary and we make no claims of optimality. This value was chosen as a trade-off between the computational cost of the search—the cost scales as the third power of the size of the basis—and the predictive power of the model. In some preliminary experiments, we found that using a larger basis did, as expected, lead to a marginally higher sensitivity to small transit signals but the gain wasn’t sufficient to justify the added cost.

4. Search pipeline

In principle, the search for transit signals simply requires evaluation of the model described above on a fine three-dimensional grid in period, phase, and duration, and then detection of high significance peaks in that space. In practice, this is computationally intractable for any grids of the required size and resolution. Instead, we can compute the values on this grid approximately, but at very high precision, using a two-step procedure that is much more efficient.

Specifically, we must evaluate the likelihood function for the light curve \mathbf{f}_n of star n

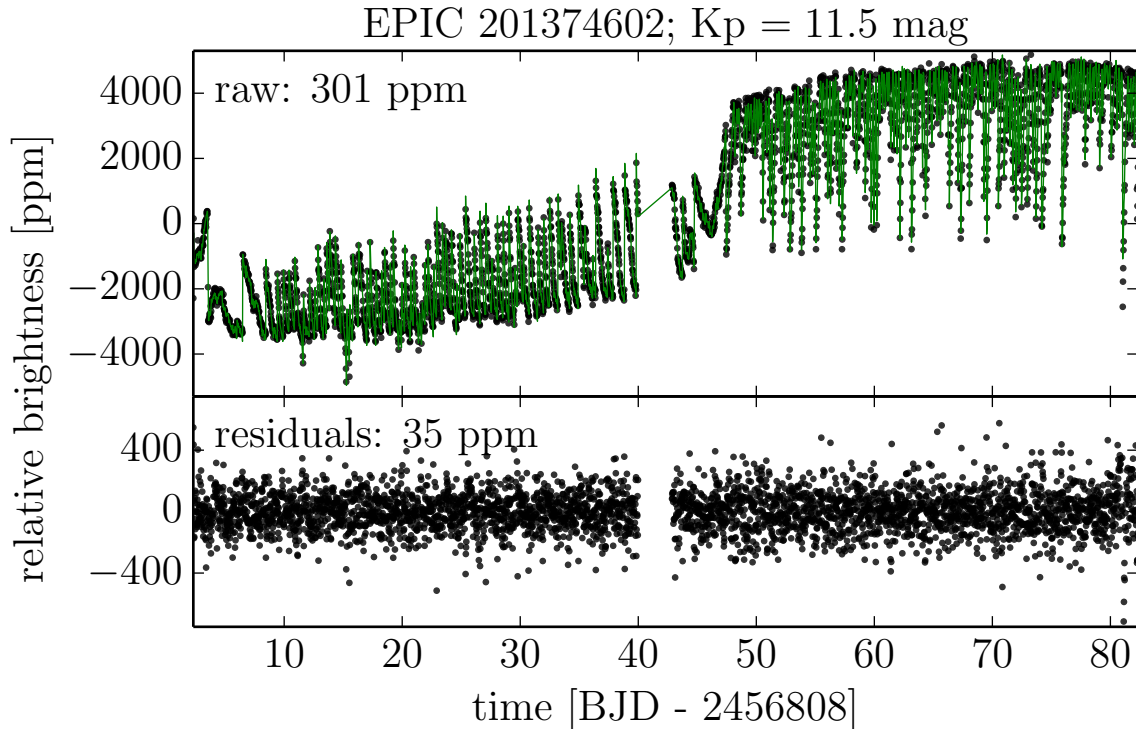


Fig. 2.— A demonstration of the eigen light curve (ELC) fit to the aperture photometry for EPIC 201374602. *Top:* The black points show the aperture photometry and the green line is the maximum likelihood linear combination of ELCs. The estimated 6-hour precision of the raw photometry is 264 ppm. *Bottom:* The points show the residuals of the data away from the ELC prediction. The 6-hour precision of this light curve is 31 ppm. Note that although we show a “de-trended” light curve to give a qualitative understanding of the model, this is not a product of the analysis. In this search for transits, *the data are only de-trended for the purpose of visualization.*

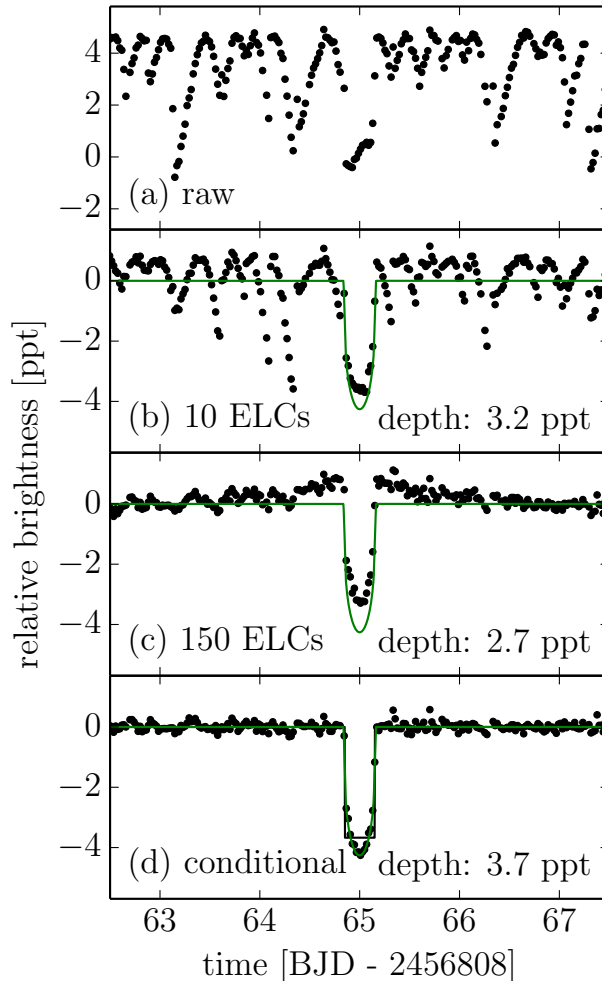


Fig. 3.— A comparison between de-trending using different numbers of ELCs and a simultaneous fit of the systematics and transit model. (a) The raw photometry for EPIC 201374602 with a synthetic transit injected at 65 days. (b) The black points show the photometry de-trended using a linear combination of 10 ELCs and the green line shows the true transit model. In this panel and the next, the maximum likelihood transit depth is computed following *BLS* (Kovács et al. 2002). While some of the systematics are removed by this model, there is still a lot of residual noise. (c) The same plot as panel (b) but using 150 ELCs to de-trend. This model removes the majority of the systematics but also distorts the transit and weakens the signal; it reduces the measured transit depth. (d) The final panel shows the results of simultaneously fitting for the transit and the systematics using 150 ELCs. The maximum likelihood depth (marginalized over the ELC weights) is computed as described in Appendix A. Like panel (c), this model removes most of the systematics but does not distort the transit or reduce the measured transit depth.

given a period P , reference transit time T^0 , duration D , and depth Z

$$p(\mathbf{f}_n | P, T^0, D, Z) \quad . \quad (1)$$

We make the simplifying assumption that each transit enters this quantity independently. This is not true; as we change beliefs about each transit, we change beliefs about the systematics model, which in turn affects the other transits. However, this simplifying assumption is approximately satisfied for all but the shortest periods and leads to a huge computational advantage. Under this assumption, this likelihood function can be rewritten as

$$p(\mathbf{f}_n | P, T^0, D, Z) = \prod_{m=1}^{M(P, T^0)} p(\mathbf{f}_n | T_m(P, T^0), D, Z) \quad (2)$$

where $T_m(P, T^0)$ is the time of the m -th transit given the period P and reference time T^0 , and $M(P, T^0)$ is the total number of transits in the dataset for the given P and T^0 . Equation (2) can be efficiently computed for many periods and phases if we first compute a set of likelihood functions for single transits on a grid in T_l and duration D_k

$$\{p(\mathbf{f}_n | T_l, D_k, Z)\}_{l=1, k=1}^{L, K} \quad . \quad (3)$$

Then, we can use these results as a look-up table—with nearest-neighbor interpolation—to approximately evaluate the full likelihood in Equation (1).

In the remainder of this Section, we give more details about each step of the search procedure. In summary, it breaks into three main steps: linear search, periodic search, and vetting. In the **linear search** step, we evaluate the likelihood function in Equation (3) on a two-dimensional grid, coarse in transit duration D_k and fine in transit time T_m . Then in the **periodic search** step, we use this two-dimensional grid to approximately evaluate the likelihood (Equation 2) for a three-dimensional grid of periodic signals. Then, we run a peak detection algorithm on this grid that is robust to signals with substantially varying transit depths. These transit candidates are then passed along for machine and human **vetting**.

Linear search The linear search requires hypothesizing a set of transit signals on a two-dimensional grid in transit time and duration. For each point in the grid, we use the model described in Section 3 to evaluate *the likelihood function* for the transit depth at that time and duration. Since the model is linear and the uncertainties are assumed Gaussian, the likelihood function for the depth (marginalized over the model of the systematics) is a Gaussian with analytic amplitude L , mean \bar{Z} , and variance $\delta\bar{Z}^2$, all derived and given in Appendix A. In the linear search, we save these three numbers on a two-dimensional grid of transit times T_l and durations D_k . The transit time grid spans the full length of Campaign 1 with half hour

spacing and we choose to only test three durations: 1.2, 2.4, and 4.8 hours. Figure 4 shows the maximum likelihood transit depth \bar{Z} as a function of transit time T for the light curve of EPIC 201613023, a transiting planet candidate with a period of 8.3 days.

Periodic search In the period search step, the table of likelihood functions generated in the linear search step are used to compute the likelihood of the periodic model (Equation 2) on a three dimensional grid in period P , reference time T^0 , and duration D . At each point in this grid, the likelihood function for each transit depth is chosen as the nearest point (without interpolation) calculated in the linear search. If the time spacing of the linear search is sufficiently fine, this will give a good approximation of the correct periodic likelihood. For each periodic model, we compute the likelihood of a model where the transit depth varies between transits and the “correct” simpler model where the transit depth is constant. The variable depth likelihood is given by the product of amplitudes from the initial search

$$p_{\text{var}}(\mathbf{f}_n | P, T^0, D) = \prod_{m=1}^{M(P, T^0)} L_m \quad . \quad (4)$$

Since the likelihood function for the depth at each transit time is known and Gaussian, the likelihood function for the depth under the periodic model can also be computed analytically; it is a product of Gaussians which itself is a Gaussian

$$p_{\text{const}}(\mathbf{f}_n | P, T^0, D) = \prod_{m=1}^{M(P, T^0)} \frac{L_m}{\sqrt{2\pi\delta\bar{Z}_m^2}} \exp\left(-\frac{[Z - \bar{Z}_m]^2}{2\delta\bar{Z}_m^2}\right) \quad (5)$$

where the maximum likelihood depth, for the periodic model, is

$$Z = \sigma_Z^2 \sum_{m=1}^{M(P, T^0)} \frac{\bar{Z}_m}{\delta\bar{Z}_m^2} \quad (6)$$

and the uncertainty is given by

$$\frac{1}{\sigma_Z^2} = \sum_{m=1}^{M(P, T^0)} \frac{1}{\delta\bar{Z}_m^2} \quad . \quad (7)$$

Note that this result has been *marginalized* over the parameters of the systematics model. Therefore, this estimate of the uncertainty on the depth takes any uncertainty that we have about the systematics into account.

In general, the variable depth model will *always* get a higher likelihood because it is more flexible. Therefore, a formal model comparison is required to compete these two

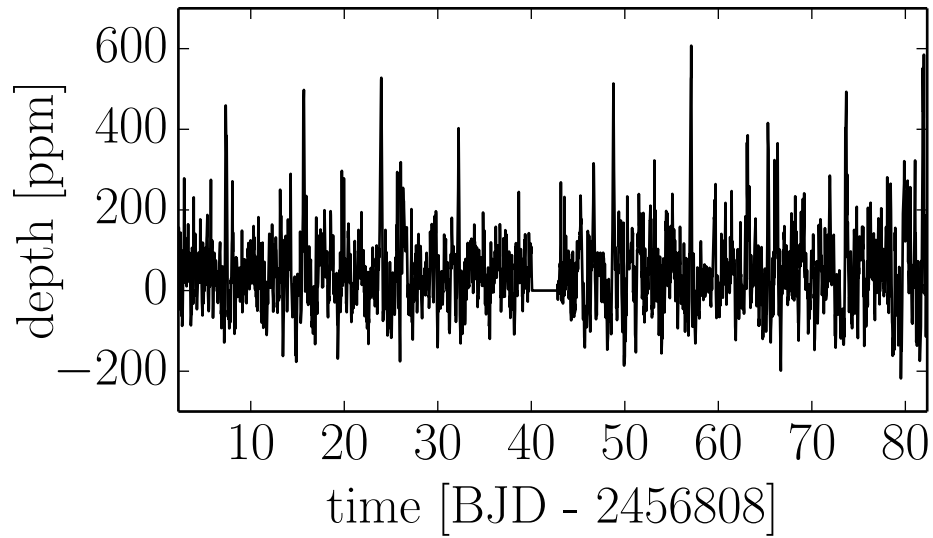


Fig. 4.— The maximum likelihood transit depth as a function of transit time as computed in the linear search of the light curve of EPIC 201613023. After the periodic search and vetting this target is found to have a planet candidate with a period of 8.3 days. The first transit occurs at 7.4 days on this plot.

models against each other on equal footing. For computational simplicity and speed, we use the Bayesian Information Criterion (BIC). The traditional definition of the BIC is

$$-\frac{1}{2} \text{BIC} = \ln p(\mathbf{f}_n | P, T^0, D) - \frac{K}{2} \ln N \quad (8)$$

where the likelihood function is evaluated at the maximum, K is an estimate of the model complexity and N is the effective sample size. To emphasize that K and N are tuning parameters of the method, we rewrite this equation as

$$-\frac{1}{2} \text{BIC} = \ln p(\mathbf{f}_n | P, T^0, D) - \frac{J\alpha}{2} \quad (9)$$

where J is the number of allowed depths—one for the constant depth model and the number of transits for the variable depth model—and α is chosen heuristically. For the K2 Campaign 1 dataset, we find that $\alpha \sim 1240$ leads to reliable recovery of injected signals while still being fairly insensitive to false signals.

To limit memory consumption, in the periodic search, we profile (or maximize) over T^0 and D subject to the constraint that $\text{BIC}_{\text{const}} < \text{BIC}_{\text{var}}$ and requiring that the signal have at least two observed transits. This yields a one-dimensional spectrum of the signal-to-noise of the depth measurement as a function of period using Equations (6) and (7) to compute Z/σ_Z at each period. The result is a generalization of the *BLS* frequency spectrum (Kovács et al. 2002) to a light curve model that includes both a transit and the trends. For example, Figure 5 shows the spectrum for a planet candidate transiting EPIC 201613023.

After selecting the best candidate based on the signal-to-noise of the depth, we mask out the sections of the linear search corresponding to these transits and iterate the periodic search. This permits us to find second transiting planets in light curves in which we have already found a more prominent signal. Under our assumption of independent transits, this masking procedure is equivalent to removing the sections of data that have a transit caused by the exoplanet that produces the highest peak. For the purposes of this *Article*, we iterate the periodic search until we find three peaks for each light curve. This will necessarily miss the smallest and longest period planets in systems with more than three transiting planets but given the conservative vetting in the next Section, three peaks are sufficient to discover all the high signal-to-noise transits.

Initial candidate list The periodic search procedure returned three signals per target so this gave an initial list of 65,109 candidates. The vast majority of these signals are not induced by a transiting planet: there are many false positives. Therefore to reduce the search space, we estimate the signal-to-noise of each candidate by comparing the peak height to a

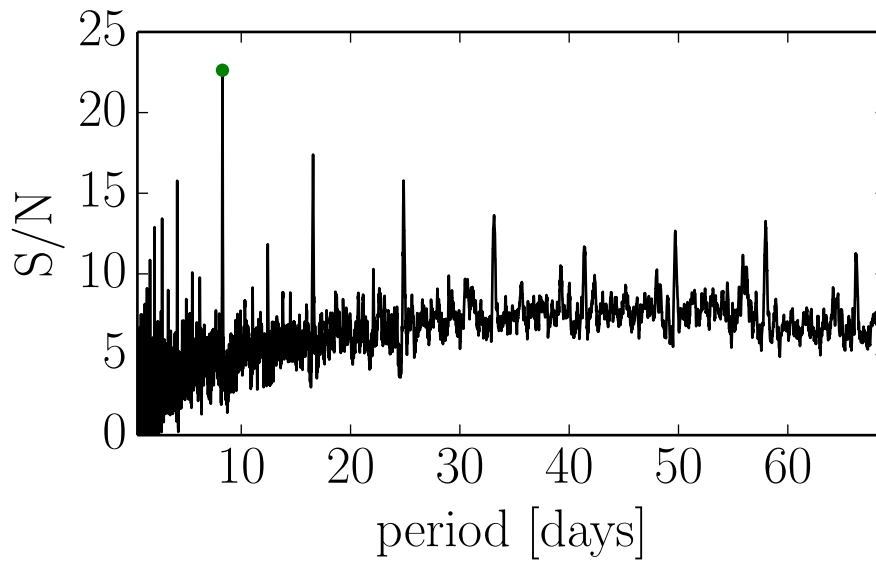


Fig. 5.— The signal-to-noise spectrum as a function of period for the light curve of EPIC 201613023. This is the generalization of the *BLS* spectrum (Kovács et al. 2002) to this simultaneous model of the transit and the systematic trends. To compute this spectrum, the results of the linear search (Figure 4) were used as described in Section 4. The top peak (at a period of 8.3 days) is indicated with a green dot. Iterating the periodic search found no other transit signals above the signal-to-noise threshold.

robust estimate of variance in BIC values across period. This is not the same criterion used to select the initial three peaks but we find that it produces a more complete and pure sample. A cut in this quantity can reject most variable stars and low signal-to-noise candidates that can't be reliably recovered from the data. To minimize contamination from false alarms but maximize our sensitivity, we choose a threshold of 15. In absolute value, this threshold is somewhat higher than the standard signal-to-noise threshold used when searching for transits in the *Kepler* light curves (for example [Petigura et al. 2013a](#)) but given the larger amplitude of the systematic noise in the *K2* light curves, it is not surprising that a higher threshold is required to produce a manageable list of candidates for hand vetting. That being said, it is likely that a reduction in this threshold would yield more discoveries at the cost of a larger set of hand classifications.

We also find that the signals with periods $\lesssim 4$ days are strongly contaminated by false alarms. This might be because of the fact that our independence assumption (Equation 2) breaks down at these short periods. Therefore, we discard all signals with periods shorter than 4 days, acknowledging this will cause us to miss some planets ([Sanchis-Ojeda et al. 2014](#)). After these cuts, 741 candidates remain; we examine these signals by hand. The full list of peaks and their relevant meta data is available online at⁵.

Hand vetting After our initial cuts on the candidate list, the majority of signals are still false alarms mostly due to variable stars or single outlying data points. It should be possible to construct a more robust machine vetting algorithm that discards these samples without missing real transits but for the purposes of this *Article*, we simply inspect the light curve for each of the 741 candidates *by hand* to discard signals that are not convincing transits. The results of this vetting can be seen online⁶.

Although de-trended light curves are never used in the automated analysis of the data, when conditioned on a specific set of transit parameters, the model produces an estimate of what the light curve would look like in the absence of systematic effects. This prediction is one of the plots that we examine when vetting candidates by hand. For example, Figure 6 shows the maximum likelihood light curve for EPIC 201613023 evaluated at the candidate period, phase, duration, and depth. Similarly, Figure 7 shows the same prediction folded on the 8.3 day period of this candidate.

After visually inspecting 741 signals, 101 candidate transits pass and are selected as

⁵<http://bbq.dfm.io/ketu>

⁶<http://bbq.dfm.io/ketu>

astrophysical events. Many of these signals are due to “false positives” such as eclipsing binary systems, either as the target star or as a background “blend.” We address this effect in the following Section, where we separate the list of candidates into a list of astrophysical false positives and planet candidates.

Astrophysical false positives A major problem with any transit search is the potential confusion between transiting planets and stellar eclipsing binaries (EBs). Of particular concern are grazing stellar eclipses or stellar eclipses that contribute only a small fraction of the total light in a photometric aperture, resulting in greatly diluted eclipse depths able to mimic the signals of small planets.

Ground-based transit surveys have experienced false-positive rates well over 50 percent. For example, [Latham et al. \(2009\)](#) reported eight eclipsing binaries and one transiting planet among the sample of transit candidates in one field of the Hungarian Automated Telescope Network transit search. In fact, the follow-up process to try to rule out such astrophysical false positives is a large portion of the effort that goes into a transit survey (e.g., [O’Donovan et al. 2006](#); [Almenara et al. 2009](#); [Poleski et al. 2010](#)).

Despite this large fraction of astrophysical false positives in ground-based surveys, the primary *Kepler* Mission saw a much lower false positive rate of only 5-10% ([Morton & Johnson 2011](#); [Fressin et al. 2013](#)), primarily due to three major factors. First, the superior precision of the *Kepler* photometry enables detection of secondary stellar eclipses, odd-even transit depth variations, and ellipsoidal variations ([Batalha et al. 2010](#)) to a much lower level than ground-based surveys. Second, the relatively small pixels and stable pointing of the *Kepler* telescope has enabled the identification of many spatially distinct blended eclipsing binaries by means of detailed pixel-level analysis ([Bryson et al. 2013](#)) to identify shifts in the center of light during transits. And finally, *Kepler* is sensitive to much smaller planets than ground-based surveys, and small planets are much more common than the Jupiter-sized planets able to be detected from the ground. We note that while [Santerne et al. \(2012\)](#) reported a $\sim 35\%$ observational false positive rate, that study was exclusively focused on short-period, large candidates, among which false positives are expected to be more likely. [Désert et al. \(2015\)](#) has observationally confirmed a low false positive rate for the majority of *Kepler* candidate parameter space.

In *K2*, the precision of the photometric tests used to vet for such false positives is lower and they must be applied with care. There are typically only a handful of transits, meaning differences between “odd” and “even” transits must be large to create a significant difference. Searching for ellipsoidal variations is hindered by the short time baseline and the increased photometric uncertainty in *K2* data. Centroid variations are feasible in *K2*

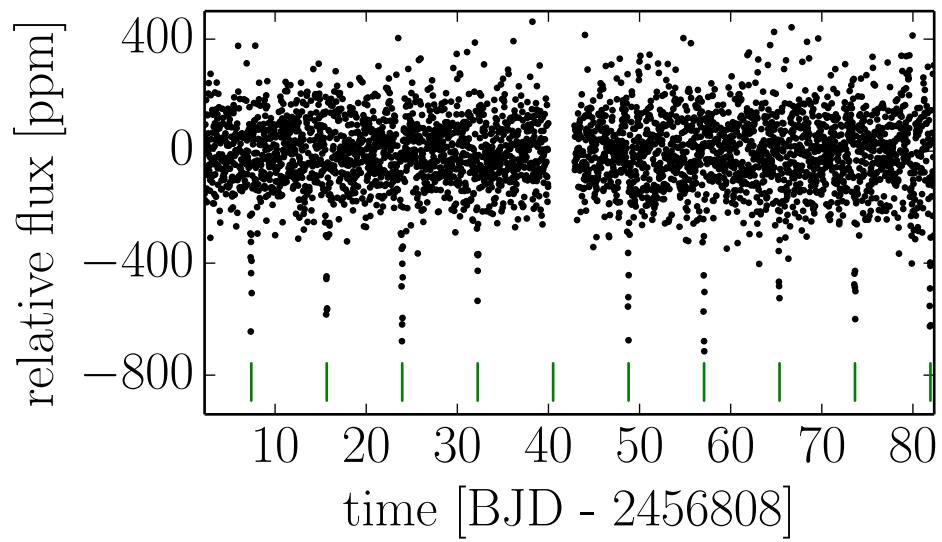


Fig. 6.— The maximum likelihood “de-trended” light curve for EPIC 201613023 evaluated at the planet candidate’s period, phase, duration, and depth. The transit times are indicated by the green ticks below the light curve. This Figure is only generated for qualitative hand vetting and in the search procedure, the model is always marginalized over any choices about the systematic trends.

but must be treated differently than in the original *Kepler* mission where this effect was generally measured using difference imaging (Batalha et al. 2010; Bryson et al. 2013).

To do first-pass vetting for blended EBs among our catalog of planetary candidates, we test for significant centroid offsets using the machinery that we have already established for modeling the systematic trends in the data, inspired by the methods used to vet *Kepler* candidates (Bryson et al. 2013). If any of the candidates have substantial centroid offsets in phase with their transits, this indicates that the signal is likely caused by a background or foreground transit of an eclipsing binary and we, therefore, remove it from the final candidate list. This is only an initial vetting step and a more complete characterization of our catalog’s reliability is forthcoming (Montet, *et al.* in preparation).

To measure *centroid offsets*, we start by empirically measuring the pixel centroid time series for each candidate by modeling the pixels near the peak as a two-dimensional quadratic and finding the maximum at each time. This method has been shown to produce higher precision centroid measurements than center-of-light estimates (Vakili *et al.*, in preparation). Figure 8 shows the measured x and y pixel coordinate traces for EPIC 201613023. Much like the photometry, this signal is dominated by the rigid body motion of the spacecraft and we can, in fact, model it identically. In our analysis, we model the light curve as a linear combination of ELCs and a simple box transit model at a given period, phase, and duration (Equation A1). Under this model, the maximum likelihood depth can be computed analytically. If we apply *exactly the same model* to the centroid trace, the “depth” that we compute becomes the centroid motion in transit in units of pixels. Since the motions won’t necessarily point in a consistent direction across transits, we treat each transit independently and report the average offset amplitude weighted by the precision of each measurement. To compute the significance of a centroid offset, we bootstrap the offset amplitude for models at the same period and duration but randomly oriented phases. If the centroid measured for the candidate transit is substantially larger than the random realizations, we label the candidate as a false positive. In practice, the precision of the centroid measurements isn’t sufficient to robustly reject many candidates, but two candidates—EPIC 201202105 and EPIC 201632708—have offsets $3\text{-}\sigma$ above the median out-of-transit offset amplitude so they are removed from the final catalog. For example, Figure 9 shows the in-transit centroid offset measured for EPIC 201202105 and compares it to the distribution of out-of-transit offset amplitudes.

A quick *a priori* estimate of the background blended eclipsing binary rate serves as a good sanity check. A query to the TRILEGAL (TRIdimensional modeL of thE GALaxy, Girardi et al. 2005) galaxy line-of-sight simulation software reveals that the typical density of field stars along the line of sight to the Campaign 1 field is about $7.8 \times 10^{-4} \text{ arcsec}^{-2}$.

This gives a probability of about 0.16 that a background star might be blended within a 8 arcsec radius (two pixels) from a target star. Allowing that $\sim 10\%$ of stars might host close binary companions within the period range accessible by this survey, this gives a probability of 0.016 that a blended binary star might be chance-aligned within two pixels of any given target star. Noting that the average number of planets per star with periods less than 30 days is about 0.25 (Fressin et al. 2013), we can roughly estimate that we expect $<10\%$ of our candidates to be caused by nearby contaminating EBs. This estimate suggests that such astrophysical false positives should be rare in our sample, consistent with our detection of only 2 candidates with clear centroid offsets.

5. Performance

To test the performance and detection efficiency of our method, we conducted a suite of injection and recovery tests, five per star for all 21,703 target stars. For each test, we inject the signal from a realistic planetary system into the raw aperture photometry of a random target and run the resulting injected light curve through the full pipeline (except the manual vetting). If the search returns a planet candidate—passing all of the same cuts as we apply in the main search (except the manual vetting)—with period and reference transit time within 6 hours of the injected signal, we count that injection as recovered. The detection efficiency of the search is given approximately by the fraction of recovered injections as a function of the relevant parameters.

To generate the synthetic signals, we use the following procedure:

1. Draw the number of transiting planets based on the observed multiplicity distribution of KOIs (Burke et al. 2014).
2. Sample—from the distributions listed in Table 1—limb darkening parameters and, for each planet, an orbital period, phase, radius ratio, impact parameter, eccentricity, and argument of periapsis.
3. Based on the chosen physical parameters, simulate the light curve, taking limb darkening and integration time into account (Mandel & Agol 2002; Kipping 2010), and multiply it into the raw aperture photometry.

We then process these light curves using exactly the pipeline that we use for the light curves without injections. Finally, we test for recovery after applying the cuts in signal-to-noise and period. We should, of course, also vet the results of the injection tests by hand to ensure

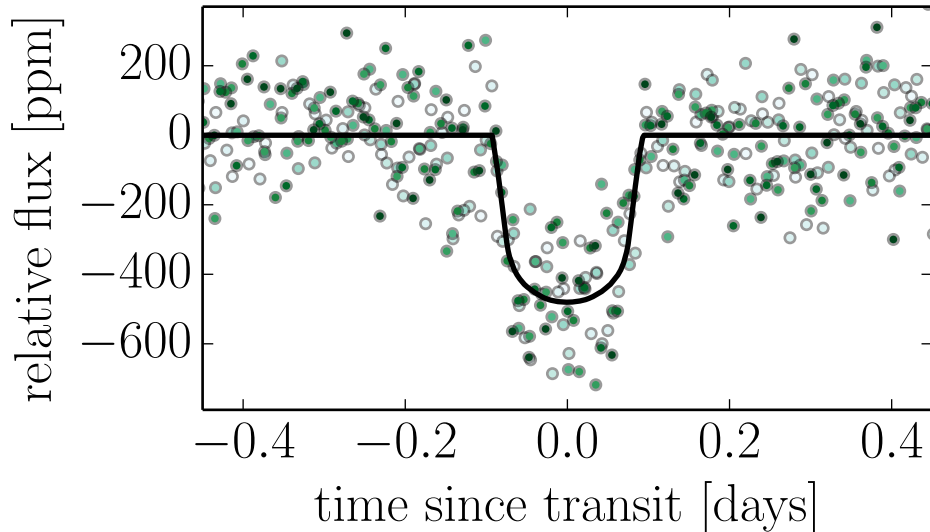


Fig. 7.— The maximum likelihood prediction for the light curve of EPIC 201613023 (see also Figure 6) folded on the 8.3 day period of this planet candidate. The points are color-coded by time and the median *a posteriori* transit model is overplotted as a black line.

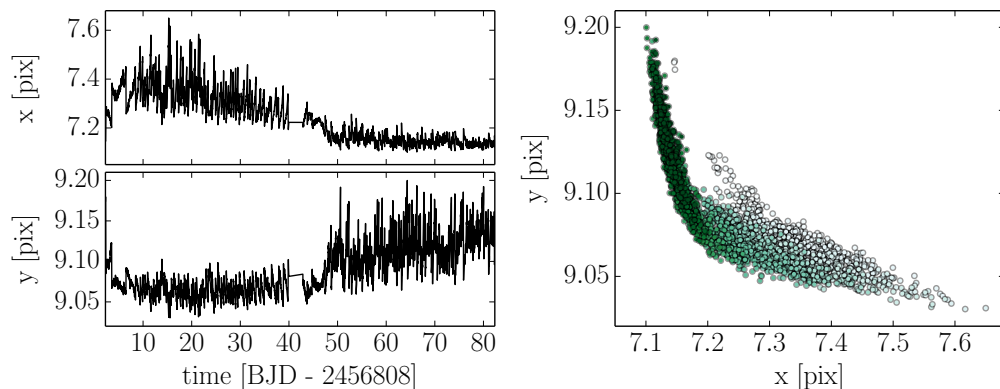


Fig. 8.— The centroid motion for EPIC 201613023. *Left:* The measured x and y pixel coordinates as a function of time. *Right:* The pixel coordinates color-coded by time. As identified by [Vanderburg & Johnson \(2014\)](#), the centroid motions fall in a slowly time variable locus. If the centroid coordinates in transit are inconsistent with the out-of-transit motions, the candidate is likely to be an astrophysical false positive.

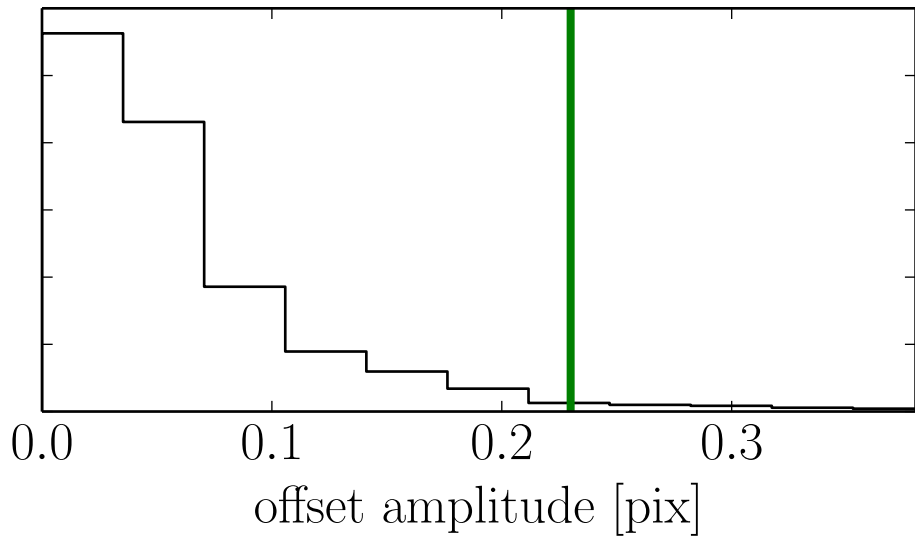


Fig. 9.— The estimated in-transit centroid offset for EPIC 201202105 (green line) compared to the distribution of 1000 centroid offsets computed for randomly assigned phases (black histogram). The in-transit measurement is $3\text{-}\sigma$ larger than the median out-of-transit offset so it is rejected from the final catalog.

that our measurements of detection efficiency aren’t biased by the hand-vetting step but, since we chose to limit our sample to very high signal-to-noise candidates, it seems unlikely that our hand vetting removed any true transit signals. Any estimates of the false alarm rate will, however, be affected by this negligence but we leave a treatment of this for future work.

Figures 10 and 11 show the fraction of recovered signals as a function of the physical parameters of the injection, and the magnitude of the star in the *Kepler* bandpass as reported in the Ecliptic Plane Input Catalog (EPIC⁷). As expected, the shallower transits at longer periods are recovered less robustly and all signals become harder to detect for fainter stars. It is worth noting that these Figures are projections (or marginalizations) of a higher dimensional measurement of the recovery rate as a function of all of the input parameters. For example, this detection efficiency map is conditioned on our assumptions about the eccentricity distribution of planets and it is marginalized over the empirical distribution of stellar parameters. It is possible to relax this assumption and apply different distributions by re-weighting the simulations used to generate this figure. Therefore, alongside this *Article*, we publish the full list of injection simulations⁸ to be used for population inference (occurrence rate measurements).

While we argue that the most relevant quantity to use to quantify the performance of a transit search pipeline is the efficiency with which it discovers transits, it is also useful to consider some other standard metrics. In particular, while de-trended light curves are never used at any stage of the analysis, our method does make a prediction for the systematics model and we can measure the relative precision of the residuals away from this model. These residuals are what would be used as de-trended light curves if that was the goal. Figure 12 shows, as a function of the *Kepler* magnitude reported in the EPIC, the 6-hour CDPP (Christiansen et al. 2012) for each light curve after subtracting the best fit linear combination of 150 ELCs.

6. Results

Out of the 21,703 Campaign 1 light curves, our pipeline returns 741 signals that pass the signal-to-noise and period cuts. After hand vetting by the two first authors, this list is reduced to 101 convincing astrophysical transit candidates. Of these, 36 signals—in 31

⁷<http://archive.stsci.edu/k2/epic.pdf>

⁸<http://bbq.dfm.io/ketu>

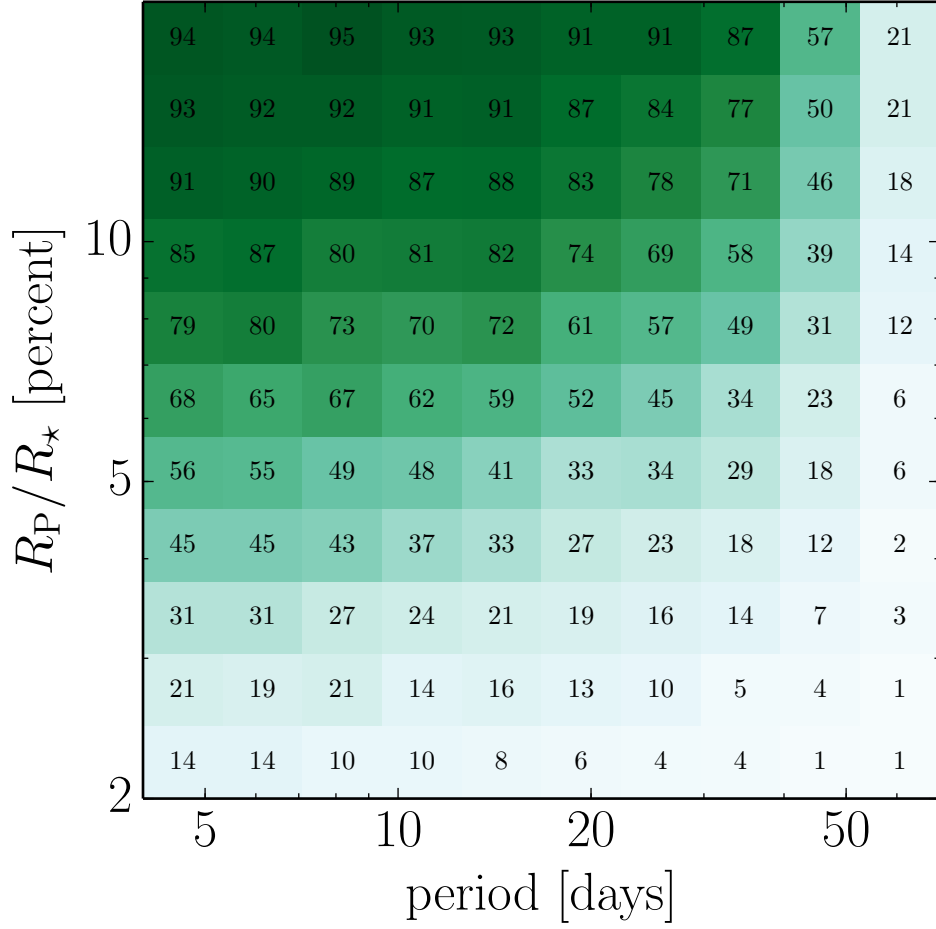


Fig. 10.— The detection efficiency of the search procedure as a function of the physical transit parameters computed empirically by injecting synthetic transit signals into the raw light curves and measuring the fraction that are successfully recovered. These tests were performed on the entire set of stars so these numbers are marginalized over all the stellar properties, including magnitude.

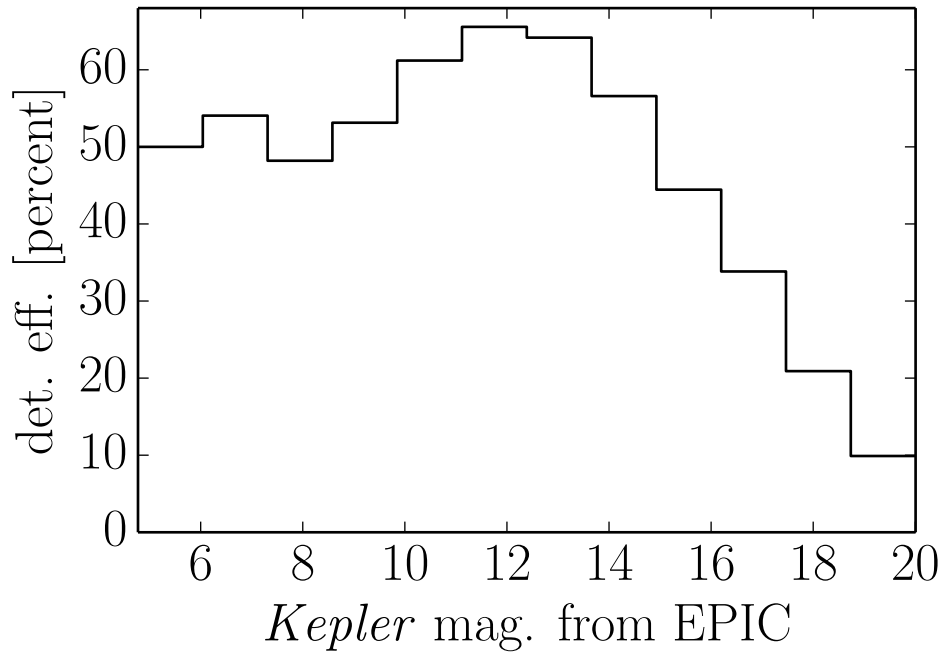


Fig. 11.— Like Figure 10, the empirically measured detection efficiency of the search procedure as a function of stellar magnitude as reported by the Ecliptic Plane Input Catalog. This never reaches 90 percent because these numbers are marginalized over the range of physical parameters shown in Figure 10. Even for the brightest stars, the long period, small transits cannot be detected.

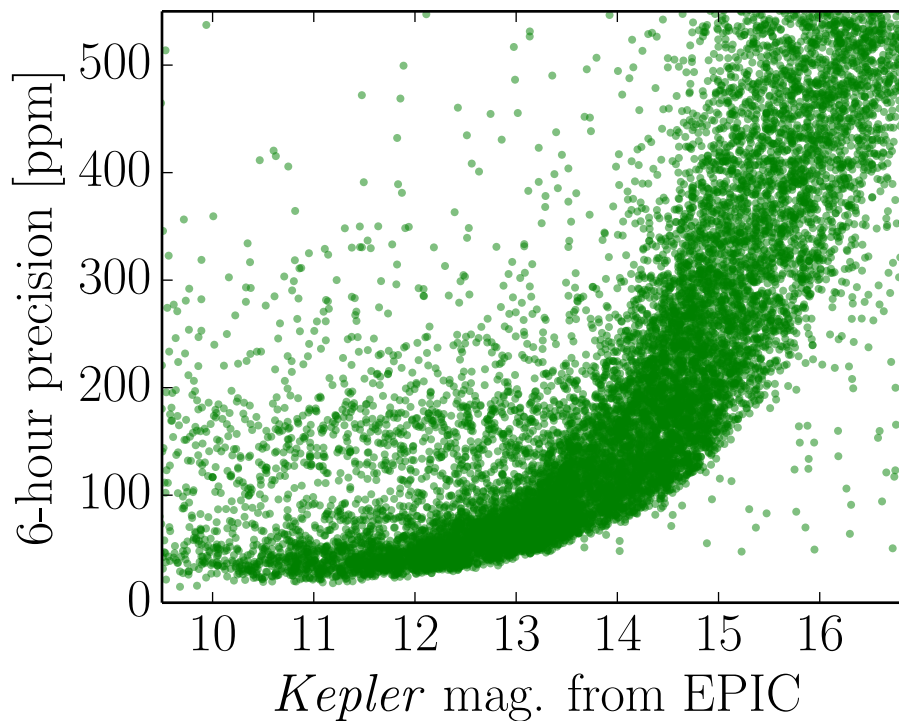


Fig. 12.— The 6-hour CDPP (Christiansen et al. 2012) for each light curve in Campaign 1 after subtracting the best fit linear combination of 150 ELCs. For each star, the precision is plotted as a function of the *Kepler* magnitude reported in the Ecliptic Plane Input Catalog. The “outliers” in the bottom right corner of the plot are caused by a bright star within the photometric aperture and the points in the top left corner of the plot are variable stars where the major trends in the light curve are not caused by systematic effects, making the ELC model a bad fit.

light curves—have no visible secondary eclipse and are deemed planet candidates. These planet candidates are listed in Table 2. The two candidates transiting EPIC 201367065 were previously published (Crossfield et al. 2015) and the third planet in that system is found as the third signal by our pipeline but it falls just below the signal-to-noise cut so it is left out of the catalog for consistency. This suggests that a less conservative cut in signal-to-noise and more aggressive machine vetting could yield a much more complete catalog at smaller radii and longer periods even with the existing dataset.

The remaining signals are caused by EBs with visible secondary eclipses. In most cases, the search reports the secondary eclipse as a candidate and in a few very high signal-to-noise cases, the period reported by the pipeline is incorrect and multiple candidates correspond to the same transit. It is important to note, however, that the choices made in the search were heuristically tuned to find planets, not binaries, so our results are not complete or exhaustive, especially at short orbital periods. There are other methods specifically tuned to find EBs in *K2* (such as Armstrong et al. 2014, 2015) and these catalogs contain our full sample of EBs and more.

For the planet candidates, we perform a full physical transit fit to the light curve. To do this fit, we use Markov Chain Monte Carlo (MCMC; Foreman-Mackey et al. 2013) to sample from the posterior probability for the stellar and planetary parameters taking limb darkening and integration time into account. In this fit, we continue to model the trends in the data as a linear combination of the 150 ELCs but, at this point, we combine this with a realistic light curve model (Mandel & Agol 2002; Kipping 2013a). Even though we have no constraints on the stellar parameters, we also sample over a large range in stellar mass and radius so that future measurements can be applied by re-weighting the published samples. In Table 2 we list the sample quantiles for the observable quantities and the full chains are available electronically⁹. Figure 13 shows the observed distribution of planet candidates in the catalog.

In a follow-up to this *Article*, we will characterize the stars for each of the candidates in detail but for now it’s worth noting that many of the planet candidates are orbiting stars selected for *K2* as M-type stars. If this rate remains robust after stellar characterization and if these numbers are representative of the yields in upcoming *K2* Campaigns, the *K2* Mission will substantially increase the number of planets known to transit cool stars.

⁹<http://bbq.dfm.io/ketu>

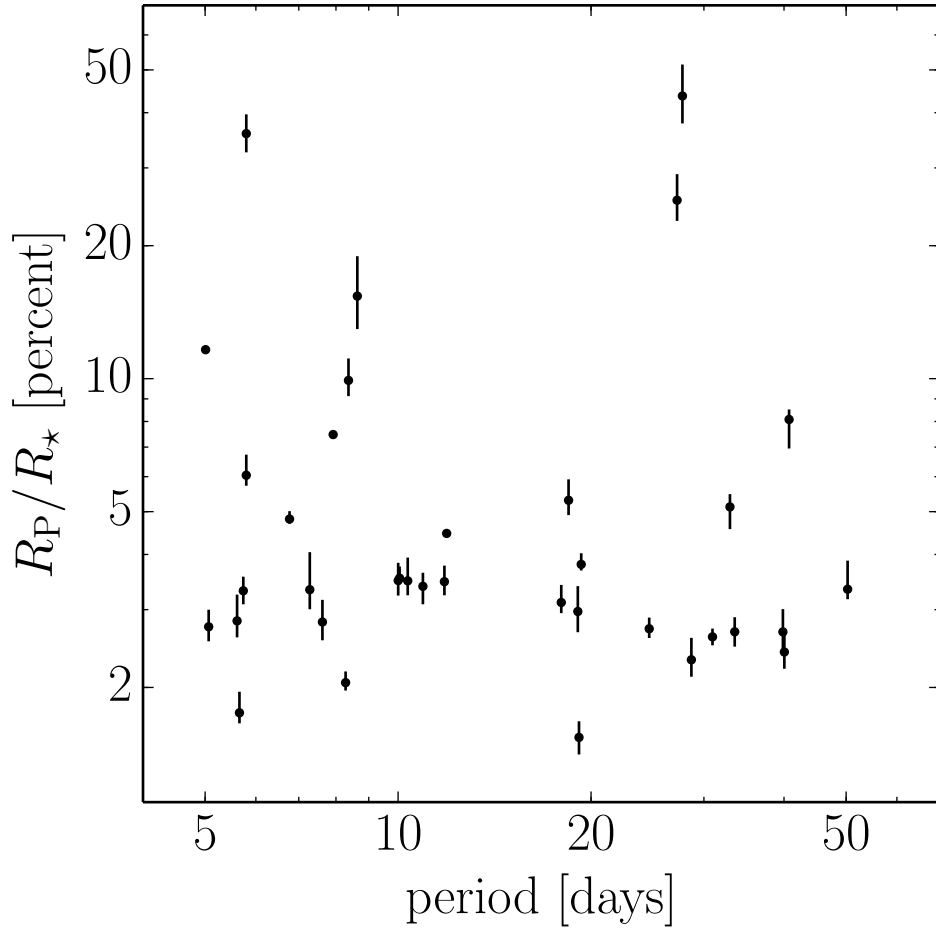


Fig. 13.— The *a posteriori* distribution of planet candidates in the catalog. The error bars indicate the 0.16 and 0.84 posterior sample quantiles for the radius ratios.

7. Discussion

We have searched the *K2* Campaign 1 data set for exoplanet transit signals. Our search is novel because it includes a very flexible systematics model, which is fit simultaneously with the exoplanet signals of interest (and marginalized out). By this method, we find 36 transiting exoplanets, which we have vetted by both automatically and manually and characterized by probabilistic modeling. The candidates are listed in Table 2 and posterior distributions of planet candidate properties are available¹⁰.

The flexible systematics model we employ is a 150-parameter linear combination of PCA components derived from the full set of 21,703 stellar light curves. That is, it presumes that the systematics afflicting each star are shared in some way across other stars while the astrophysical signals are causally unconnected (Schölkopf et al. 2015). This assumption means that, while there is no formal guarantee that the basis contains no astrophysical signals, it is unlikely that the top components will be contaminated. It is our belief—although not a strict assumption of our model—that the systematics are caused primarily by pointing drifts, or movements of the pixels in the focal plane relative to the stars. In principle, if the systematics *are* dominated by pointing issues, the systematics model could require only three parameters—three Euler angles—not 150 amplitudes. However, because (as the pointing drifts) each star sees its own unique local patch of flat-field variations, the mapping from pointing drifts to brightness variations can be extremely non-linear. Furthermore, because when the pointing is moving fast there is a smearing of the point-spread function, there are effects keyed to the time derivative of the Euler angles as well. The large number (150) of linear coefficients gives the linear model the freedom to model complex non-linear behavior; we are trading off parsimony in parameters with the enormous computational advantages of maintaining linearity (and therefore also convexity). The computational advantages of the linear model are three-fold: Convexity obviates searching in parameter space for alternative modes; linear least-squares optimization can be performed with simple linear algebra; given Gaussian uncertainties and uninformative priors, marginalizations over the linear parameters also reduces to pure linear algebra.

The goal of this *Article* was to get exoplanet candidates out of the *K2* pixel-level data, it was *not* to generate light curves. That is, both the search phase and the characterization phase of the method are approximations to computations of a likelihood function for the pixel data telemetered down from the satellite. We did not generate “corrected” or “pre-search conditioned” light-curves at any stage; we simultaneously fit systematics and the signals of interest to the raw data. For this reason, there is no sense in which this method ever really

¹⁰<http://bbq.dfm.io/ketu>

produces corrected light curves.

In this work, we are agnostic about fundamental properties of the host stars. The only assumptions we make are that the star targeted by the *K2* team is truly the planet host, and that there is no dilution by other stars in any aperture. As a result, these posterior distributions reflect the maximum possible uncertainty in parameters such as the planet radius, which depend sensitively on properties of the host star. To use these distributions to characterize the properties of specific systems, one could re-weight our samples using a measurement of the inferred stellar properties.

This project does not live in isolation and this is certainly not the last time the *K2* data will be searched! There are other teams searching the *K2* light curves for transiting planets (A. Vanderburg, private comm.) and they are likely to find some planets that we did not and vice versa. We make many heuristic choices and short-cuts in this search. For example, the choice to work at 150 principal components was based on computational feasibility and qualitative tests on a handful of light curves instead of any real model selection or utility optimization.

Another major limitation is that, in principle, the systematics model is designed to describe spacecraft-induced trends, but not intrinsic stellar variability. In practice, the method can still find planets around variable stars but a more sophisticated model should be more robust in this case. One appealing option would be to model the systematics as a Gaussian Process where the input parameters are both time and the same 150 ELCs. Interestingly, while this model isn't linear, the search and marginalization can still be executed efficiently—using optimized linear algebra algorithms (Ambikasaran et al. 2014, Foreman-Mackey et al. in preparation)—inside the search loop.

Additionally, while we apply this systematics model simultaneously with a transiting planet model to search for planet candidates, this scheme is not restricted to planet searches. Any astrophysical event that could be observed in the *K2* data could be searched for in the same way. By modeling a set of ELCs with any arbitrary data model, events in the *K2* data that appear similar to that data model could be identified. Such a technique may be useful in searching for astrophysical events such as ellipsoidal variations induced by orbiting companions, stellar activity, microlensing events, especially in the upcoming Campaign 9, or active galactic nuclei variability.

A substantial caveat to the reliability of all existing transiting exoplanet searches is that they all include human intervention. This makes quantifying the false alarm rate of these catalogs complicated. There has been some work on automated vetting algorithms using supervised classification algorithms (McCauliff et al. 2014; Jenkins et al. 2014) but

these methods rely on hand classified examples for training and the performance is not yet competitive with human classification.

The catalog of planet candidates presented here includes only planets with periods longer than 4 days and at least two transits in the *K2* Campaign 1 footprint. This means that we are necessarily missing many planets with orbital periods outside this range. In particular, planets with a single transit in the dataset must be abundant. These candidates are the most relevant for the study of planetary system formation and for statistical inference of the distribution of habitable zone exoplanets. What’s more, given the observing strategy for *TESS*, where each field will only be contiguously observed for one month at a time, methods for finding and characterizing planets with a single transit are vital and the new *K2* light curves are a perfect test bed.

As a supplement to this *Article*, we make all the results, data products, and MCMC chains available at <http://bbq.dfm.io/ketu>. The L^AT_EX source for this *Article*, complete with the full revision history, is available at <http://github.com/dfm/k2-paper> and the pipeline implementation is available at <http://github.com/dfm/ketu> under the MIT open-source software license. This code and a lot of computation time are all that is needed to reproduce the Figures in this *Article*.

It is a pleasure to thank Eric Agol (UW), Ruth Angus (Oxford), Tom Barclay (Ames), Zach Berta-Thompson (MIT), Daniel Bramich (QEERI, Qatar), Géza Kovács (Konkoly Observatory), Laura Kreidberg (Chicago), Erik Petigura (Berkeley), Roberto Sanchis Ojeda (Berkeley), and Andrew Vanderburg (Harvard) for helpful contributions to the ideas and code presented here. We also thank the anonymous referee for comments that improved the manuscript. DFM, DWH, and DW were partially supported by the National Science Foundation (grant IIS-1124794), the National Aeronautics and Space Administration (grant NNX12AI50G), and the Moore–Sloan Data Science Environment at NYU. BTM was supported by a National Science Foundation Graduate Research Fellowship (grant DGE1144469).

This research made use of the NASA *Astrophysics Data System* and the NASA Exoplanet Archive. The Archive is operated by the California Institute of Technology, under contract with NASA under the Exoplanet Exploration Program. This *Article* includes data collected by the *Kepler* mission. Funding for the *Kepler* mission is provided by the NASA Science Mission directorate. We are grateful to the entire *Kepler* team, past and present. Their tireless efforts were all essential to the tremendous success of the mission and the successes of *K2*, present and future. These data were obtained from the Mikulski Archive for Space Telescopes (MAST). STScI is operated by the Association of Universities for Research

in Astronomy, Inc., under NASA contract NAS5-26555. Support for MAST is provided by the NASA Office of Space Science via grant NNX13AC07G and by other grants and contracts.

Facilities: Kepler

A. Mathematical model

We model the raw aperture photometry as a linear combination of 150 ELCs and a transit model. Formally, this can be written for the light curve of the k -th star as

$$\mathbf{f}_k = \mathbf{A} \mathbf{w}_k + \text{noise} \quad (\text{A1})$$

where

$$\mathbf{f}_k = \left(f_{k,1} \ f_{k,2} \ \cdots \ f_{k,N} \right)^T \quad (\text{A2})$$

is the list of aperture fluxes for star k observed at N times

$$\mathbf{t} = \left(t_1 \ t_2 \ \cdots \ t_N \right)^T . \quad (\text{A3})$$

In Equation (A1), the design matrix is given by

$$\mathbf{A} = \begin{pmatrix} x_{1,1} & x_{2,1} & \cdots & x_{150,1} & 1 & m_{\boldsymbol{\theta}}(t_1) \\ x_{1,2} & x_{2,2} & \cdots & x_{150,2} & 1 & m_{\boldsymbol{\theta}}(t_2) \\ & & \vdots & & & \\ x_{1,N} & x_{2,N} & \cdots & x_{150,N} & 1 & m_{\boldsymbol{\theta}}(t_N) \end{pmatrix} \quad (\text{A4})$$

where the $x_{j,n}$ are the basis ELCs—with the index j running over components and the index n running over time—and $m_{\boldsymbol{\theta}}(t)$ is the transit model

$$m_{\boldsymbol{\theta}}(t) = \begin{cases} -1 & \text{if } t \text{ in transit} \\ 0 & \text{otherwise} \end{cases} \quad (\text{A5})$$

parameterized by a period, phase, and transit duration (these parameters are denoted by $\boldsymbol{\theta}$).

Assuming that the uncertainties on \mathbf{f}_k are Gaussian and constant, the maximum likelihood solution for \mathbf{w} is

$$\mathbf{w}_k^* \leftarrow (\mathbf{A}^T \mathbf{A})^{-1} \mathbf{A}^T \mathbf{f}_k \quad (\text{A6})$$

and the marginalized likelihood function for the transit depth is a Gaussian with the mean given by the last element of \mathbf{w}_k^* and the variance given by the lower-right element of the matrix

$$\delta \mathbf{w}_k^2 \leftarrow \sigma_k^2 (\mathbf{A}^\top \mathbf{A})^{-1} \quad (\text{A7})$$

where σ_k is the uncertainty on \mathbf{f}_k . The amplitude of this Gaussian is given by

$$\mathcal{L}_k = \frac{1}{(2\pi\sigma_k^2)^{N/2}} \exp\left(-\frac{1}{2\sigma_k^2} |\mathbf{f}_k - \mathbf{A}\mathbf{w}_k^*|^2\right) \quad (\text{A8})$$

evaluated at the maximum likelihood value \mathbf{w}_k^* .

REFERENCES

- Aigrain, S., Hodgkin, S. T., Irwin, M. J., Lewis, J. R., & Roberts, S. J. 2015, *MNRAS*, 447, 2880
- Almenara, J. M., Deeg, H. J., Aigrain, S., et al. 2009, *A&A*, 506, 337
- Ambikasaran, S., Foreman-Mackey, D., Greengard, L., Hogg, D. W., & O’Neil, M. 2014, ArXiv e-prints, arXiv:1403.6015
- Armstrong, D. J., Osborn, H. P., Brown, D. J. A., et al. 2014, ArXiv e-prints, arXiv:1411.6830
- Armstrong, D. J., Kirk, J., Lam, K. W. F., et al. 2015, ArXiv e-prints, arXiv:1502.04004
- Barclay, T., Rowe, J. F., Lissauer, J. J., et al. 2013, *Nature*, 494, 452
- Batalha, N. M., Rowe, J. F., Gilliland, R. L., et al. 2010, *ApJ*, 713, L103
- Berta, Z. K., Irwin, J., Charbonneau, D., Burke, C. J., & Falco, E. E. 2012, *AJ*, 144, 145
- Bryson, S. T., Jenkins, J. M., Gilliland, R. L., et al. 2013, *PASP*, 125, 889
- Burke, C. J., Bryson, S. T., Mullally, F., et al. 2014, *ApJS*, 210, 19
- Christiansen, J. L., Jenkins, J. M., Caldwell, D. A., et al. 2012, *PASP*, 124, 1279
- Crossfield, I. J. M., Petigura, E., Schlieder, J., et al. 2015, ArXiv e-prints, arXiv:1501.03798
- Désert, J.-M., Charbonneau, D., Torres, G., et al. 2015, ArXiv e-prints, arXiv:1503.03173
- Dressing, C. D., & Charbonneau, D. 2015, ArXiv e-prints, arXiv:1501.01623
- Foreman-Mackey, D., Hogg, D. W., Lang, D., & Goodman, J. 2013, *PASP*, 125, 306
- Foreman-Mackey, D., Hogg, D. W., & Morton, T. D. 2014, *ApJ*, 795, 64
- Fressin, F., Torres, G., Charbonneau, D., et al. 2013, *ApJ*, 766, 81
- Gilliland, R. L., Chaplin, W. J., Dunham, E. W., et al. 2011, *ApJS*, 197, 6
- Girardi, L., Groenewegen, M. A. T., Hatziminaoglou, E., & da Costa, L. 2005, *A&A*, 436, 895
- Howell, S. B., Sobeck, C., Haas, M., et al. 2014, *PASP*, 126, 398

- Jenkins, J. M., McCauliff, S., Burke, C., et al. 2014, in IAU Symposium, Vol. 293, IAU Symposium, ed. N. Haghhighipour, 94–99
- Kipping, D. M. 2010, MNRAS, 408, 1758
- . 2013a, MNRAS, 435, 2152
- . 2013b, MNRAS, 434, L51
- Kovács, G., Bakos, G., & Noyes, R. W. 2005, MNRAS, 356, 557
- Kovács, G., Zucker, S., & Mazeh, T. 2002, A&A, 391, 369
- Latham, D. W., Bakos, G. Á., Torres, G., et al. 2009, ApJ, 704, 1107
- Mandel, K., & Agol, E. 2002, ApJ, 580, L171
- McCauliff, S., Jenkins, J. M., Catanzarite, J., et al. 2014, ArXiv e-prints, arXiv:1408.1496
- Morton, T. D., & Johnson, J. A. 2011, ApJ, 738, 170
- O’Donovan, F. T., Charbonneau, D., Torres, G., et al. 2006, ApJ, 644, 1237
- Ofir, A., Alonso, R., Bonomo, A. S., et al. 2010, MNRAS, 404, L99
- Petigura, E. A., Howard, A. W., & Marcy, G. W. 2013a, Proceedings of the National Academy of Science, 110, 19273
- Petigura, E. A., Marcy, G. W., & Howard, A. W. 2013b, ApJ, 770, 69
- Poleski, R., McCullough, P. R., Valenti, J. A., et al. 2010, ApJS, 189, 134
- Ricker, G. R., Winn, J. N., Vanderspek, R., et al. 2014, in Society of Photo-Optical Instrumentation Engineers (SPIE) Conference Series, Vol. 9143, Society of Photo-Optical Instrumentation Engineers (SPIE) Conference Series, 20
- Sanchis-Ojeda, R., Rappaport, S., Winn, J. N., et al. 2014, ApJ, 787, 47
- Santerne, A., Díaz, R. F., Moutou, C., et al. 2012, A&A, 545, A76
- Schölkopf, B., Hogg, D. W., Wang, D., et al. 2015, Proceedings of the 32nd International Conference on Machine Learning, (in press)
- Smith, J. C., Stumpe, M. C., Van Cleve, J. E., et al. 2012, PASP, 124, 1000
- Stumpe, M. C., Smith, J. C., Van Cleve, J. E., et al. 2012, PASP, 124, 985

Tamuz, O., Mazeh, T., & Zucker, S. 2005, MNRAS, 356, 1466

Vanderburg, A., & Johnson, J. A. 2014, PASP, 126, 948

Vanderburg, A., Montet, B. T., Johnson, J. A., et al. 2014, ArXiv e-prints, arXiv:1412.5674

Wang, D., Foreman-Mackey, D., Hogg, D. W., & Schölkopf, B. 2015, in American Astronomical Society Meeting Abstracts, Vol. 225, American Astronomical Society Meeting Abstracts, 258.08

Parameter	Units	Distribution
limb darkening parameters q_1 and q_2	—	$q \sim U(0, 1)$
orbital period P	days	$\ln P \sim U(\ln 0.5, \ln 70)$
reference transit time T^0	days	$T^0 \sim U(0, P)$
radius ratio R_P/R_\star	—	$\ln R_P/R_\star \sim U(\ln 0.02, \ln 0.2)$
impact parameter b	—	$b \sim U(0, 1)$
eccentricity e	—	$e \sim \text{Beta}(0.867, 3.03)$
argument of periapsis ω	—	$\omega \sim U(-\pi, \pi)$

Table 1: The distribution of physical parameters for the injected signals. The eccentricity distribution is based on [Kipping \(2013b\)](#) and the limb darkening parameterization is given by [Kipping \(2013a\)](#).

EPIC	Kepler mag	RA (J2000)	Dec (J2000)	P [days]	t_0 [BJD-2456808]	R_p/R_*
201208431	14.41	174.745640	-3.905585	10.0040 ^{+0.0018} _{-0.0016}	7.5216 ^{+0.0098} _{-0.0090}	0.0349 ^{+0.0034} _{-0.0026}
201257461	11.51	178.161109	-3.094936	50.2677 ^{+0.0083} _{-0.0074}	20.3735 ^{+0.0147} _{-0.0098}	0.0334 ^{+0.0054} _{-0.0017}
201295312	12.13	174.011630	-2.520881	5.6562 ^{+0.0007} _{-0.0007}	3.7228 ^{+0.0086} _{-0.0091}	0.0175 ^{+0.0020} _{-0.0009}
201338508	14.36	169.303502	-1.877976	10.9328 ^{+0.0022} _{-0.0021}	6.5967 ^{+0.0088} _{-0.0081}	0.0339 ^{+0.0025} _{-0.0030}
201338508	14.36	169.303502	-1.877976	5.7350 ^{+0.0006} _{-0.0006}	0.8626 ^{+0.0054} _{-0.0055}	0.0331 ^{+0.0025} _{-0.0023}
201367065	11.57	172.334949	-1.454787	10.0542 ^{+0.0004} _{-0.0004}	5.4186 ^{+0.0018} _{-0.0018}	0.0354 ^{+0.0022} _{-0.0011}
201367065	11.57	172.334949	-1.454787	24.6470 ^{+0.0014} _{-0.0016}	4.2769 ^{+0.0030} _{-0.0029}	0.0272 ^{+0.0016} _{-0.0013}
201384232	12.51	178.192260	-1.198477	30.9375 ^{+0.0029} _{-0.0052}	19.5035 ^{+0.0053} _{-0.0039}	0.0260 ^{+0.0011} _{-0.0011}
201393098	13.05	167.093771	-1.065755	28.6793 ^{+0.0105} _{-0.0116}	16.6212 ^{+0.0305} _{-0.0177}	0.0231 ^{+0.0028} _{-0.0020}
201403446	11.99	174.266344	-0.907261	19.1535 ^{+0.0050} _{-0.0050}	7.3437 ^{+0.0116} _{-0.0143}	0.0154 ^{+0.0014} _{-0.0013}
201445392	14.38	169.793665	-0.284375	10.3527 ^{+0.0011} _{-0.0011}	5.6110 ^{+0.0047} _{-0.0059}	0.0349 ^{+0.0045} _{-0.0025}
201445392	14.38	169.793665	-0.284375	5.0644 ^{+0.0006} _{-0.0006}	5.0690 ^{+0.0059} _{-0.0064}	0.0274 ^{+0.0025} _{-0.0020}
201465501	14.96	176.264468	0.005301	18.4488 ^{+0.0015} _{-0.0015}	14.6719 ^{+0.0035} _{-0.0032}	0.0531 ^{+0.0061} _{-0.0039}
201505350	12.81	174.960319	0.603575	11.9069 ^{+0.0005} _{-0.0004}	9.2764 ^{+0.0013} _{-0.0015}	0.0446 ^{+0.0009} _{-0.0006}
201505350	12.81	174.960319	0.603575	7.9193 ^{+0.0001} _{-0.0001}	5.3840 ^{+0.0006} _{-0.0008}	0.0747 ^{+0.0016} _{-0.0013}
201546283	12.43	171.515165	1.230738	6.7713 ^{+0.0001} _{-0.0001}	4.8453 ^{+0.0012} _{-0.0011}	0.0481 ^{+0.0020} _{-0.0012}
201549860	13.92	170.103081	1.285956	5.6083 ^{+0.0005} _{-0.0006}	4.1195 ^{+0.0045} _{-0.0047}	0.0283 ^{+0.0041} _{-0.0023}
201555883	15.06	176.075940	1.375947	5.7966 ^{+0.0002} _{-0.0002}	5.3173 ^{+0.0027} _{-0.0050}	0.0604 ^{+0.0068} _{-0.0032}
201565013	16.91	176.992193	1.510249	8.6381 ^{+0.0003} _{-0.0002}	3.4283 ^{+0.0016} _{-0.0015}	0.1538 ^{+0.0355} _{-0.0243}
201569483	11.77	167.171299	1.577513	5.7969 ^{+0.0000} _{-0.0000}	5.3130 ^{+0.0002} _{-0.0003}	0.3587 ^{+0.0379} _{-0.0334}
201577035	12.30	172.121957	1.690636	19.3062 ^{+0.0013} _{-0.0013}	11.5790 ^{+0.0025} _{-0.0027}	0.0380 ^{+0.0023} _{-0.0012}
201596316	13.15	169.042002	1.986840	39.8415 ^{+0.0136} _{-0.0155}	21.8572 ^{+0.0120} _{-0.0101}	0.0267 ^{+0.0034} _{-0.0022}
201613023	12.14	173.192036	2.244884	8.2818 ^{+0.0006} _{-0.0007}	7.3752 ^{+0.0055} _{-0.0052}	0.0205 ^{+0.0012} _{-0.0008}
201617985	14.11	179.491659	2.321476	7.2823 ^{+0.0007} _{-0.0008}	4.6337 ^{+0.0050} _{-0.0050}	0.0333 ^{+0.0072} _{-0.0032}
201629650	12.73	170.155528	2.502696	40.0492 ^{+0.0186} _{-0.0259}	4.5363 ^{+0.0202} _{-0.0172}	0.0241 ^{+0.0025} _{-0.0020}
201635569	15.55	178.057026	2.594245	8.3681 ^{+0.0002} _{-0.0002}	3.4514 ^{+0.0015} _{-0.0014}	0.0991 ^{+0.0120} _{-0.0078}
201649426	13.22	177.234262	2.807619	27.7704 ^{+0.0001} _{-0.0001}	13.3476 ^{+0.0001} _{-0.0002}	0.4365 ^{+0.0777} _{-0.0583}
201702477	14.43	175.240794	3.681584	40.7365 ^{+0.0026} _{-0.0025}	3.5451 ^{+0.0026} _{-0.0025}	0.0808 ^{+0.0043} _{-0.0114}
201736247	14.40	178.110797	4.254747	11.8106 ^{+0.0016} _{-0.0019}	3.8483 ^{+0.0093} _{-0.0071}	0.0347 ^{+0.0030} _{-0.0024}
201754305	14.30	175.097258	4.557340	19.0726 ^{+0.0048} _{-0.0049}	1.4893 ^{+0.0128} _{-0.0133}	0.0297 ^{+0.0042} _{-0.0030}
201754305	14.30	175.097258	4.557340	7.6202 ^{+0.0012} _{-0.0011}	3.6813 ^{+0.0061} _{-0.0057}	0.0281 ^{+0.0034} _{-0.0026}
201779067	11.12	168.542699	4.988131	27.2429 ^{+0.0001} _{-0.0001}	12.2599 ^{+0.0002} _{-0.0003}	0.2535 ^{+0.0369} _{-0.0259}
201828749	11.56	175.654342	5.894323	33.5093 ^{+0.0023} _{-0.0018}	5.1554 ^{+0.0037} _{-0.0032}	0.0267 ^{+0.0021} _{-0.0020}
201855371	13.00	178.329775	6.412261	17.9715 ^{+0.0015} _{-0.0017}	9.9412 ^{+0.0033} _{-0.0038}	0.0311 ^{+0.0030} _{-0.0017}
201912552	12.47	172.560460	7.588391	32.9410 ^{+0.0039} _{-0.0032}	28.1834 ^{+0.0057} _{-0.0105}	0.0513 ^{+0.0035} _{-0.0056}
201929294	12.97	174.656969	7.959611	5.0084 ^{+0.0001} _{-0.0001}	4.5703 ^{+0.0022} _{-0.0012}	0.1163 ^{+0.0011} _{-0.0014}

Table 2: The catalog of planet candidates and their observable properties. These values and their uncertainties are derived from MCMC samplings and the numbers are computed as the 0.16, 0.5, and 0.84 posterior sample quantiles. The coordinates are retrieved directly from the EPIC.